Available online at www.sciencedirect.com
ScienceDirect
Journal of Sound and Vibration 302 (2007) 841–864
JOURNAL OF SOUND AND VIBRATION
www.elsevier.com/locate/jsvi

An analysis of the modified Dahl and Masing models: Application to a belt tensioner

Jérôme Bastien[a], Guilhem Michon[b], Lionel Manin[c,*], Régis Dufour[c]

[a]*Laboratoire Mécatronique 3M, Équipe d'accueil A 3318, Université de Technologie de Belfort-Montbéliard, 90010 Belfort Cedex, France*
[b]*Valeo Electrical Systems, 2 rue A. Boulle, 94000 Creteil, France*
[c]*LaMCoS, INSA-Lyon, CNRS UMR5259, F69621, France*

Received 20 January 2006; received in revised form 5 October 2006; accepted 6 December 2006
Available online 16 February 2007

Abstract

The objective of this paper is to describe the modified Dahl and Masing models used for predicting hysteretic behavior, and tested on a belt tensioner for automotive engines. An experimental study with deflection imposed on the tensioner is first carried out to identify hysteresis loop parameters for the two models. The models are implemented in the general motion equations which govern the behavior of a belt–tensioner–mass system. Particular attention is paid to the use of numerical schemes. The numerical and experimental investigations show the reliability of the modified Dahl model.

1. Introduction

The hysteresis behavior of components permits efficient passive control of mechanical systems but makes response prediction delicate due to their high nonlinearity [1,2]: basically it is necessary to choose an efficient hysteresis model associated with a numerical integration method to ensure convergence with the scheme. Therefore, there is a much of scientific and technological research devoted to the investigation of such problems.

Vestroni and Noori in Ref. [2] and Visintin in Ref. [3] established an overview of hysteresis models. Among the latter mention can be made of those of Bouc and Wen, Bader and Noori, and Masing. Rheological models and restoring force models are the two main categories widely used in mechanical engineering. The former provide damping and stiffness parameters, while the latter provide a restoring force to be introduced in the second member of the equations.

Let the Masing model (MM) [4,5] and the modified Dahl model (MDM) proposed by Al Majid [6,7] be the rheological and restoring force models, respectively, selected for the current analysis. The classical MM is composed of a spring parallel to a spring–dry friction system, but in this study a viscous damping element is added. The MDM originates from the Dahl and Duhem models and is based on a first differential equation

*Corresponding author.
E-mail addresses: jerome.bastien@utbm.fr (J. Bastien), guilhem.michon@valeo.com (G. Michon), lionel.manin@insa-lyon.fr (L. Manin), regis.dufour@insa-lyon.fr (R. Dufour).

0022-460X/$ - see front matter
doi:10.1016/j.jsv.2006.12.013

that provides the time derivative of the restoring force from the velocity of the deflection and from the envelop curves of the hysteresis loop. The MM is governed by a non-smooth differential equation containing a multi-valued function while the Dahl model is governed by a smooth nonlinear dynamic equation. Consequently, the numerical integration schemes have to take into account these two typical characteristics to obtain a convergence. The reliability of these two hysteresis models have to be tested to predict the hysteretic behavior of a belt tensioner.

Tensioners used in belt drive systems play a predominant role in the dynamic behavior of the belt: they maintain nominal tension in the slack span and reduce transverse vibration levels, see Ref. [8]. Tensioners often require complicated designs in order to satisfy technological challenges, see for example Ref. [9]. This type of design leads to considerably nonlinear behavior mainly due to stick–slip motion [10].

The MDM and MM are described in detail in Section 2 and then applied to a belt tensioner of an automotive engine in Section 3, where an initial experimental setup is used for identifying the model parameters. Section 4 concerns the numerical and experimental investigations performed on a belt–tensioner–mass system in which tensioner behavior is described by the two models studied. This section permits comparing the predicted and measured harmonic responses in order to discuss model reliability.

2. The models

In this section, two models describing the hysteretic behavior of a one degree of freedom mechanical system are presented. The behavior of the mechanical system studied can be analyzed via the progression of the restoring force versus the deflection, as presented in Fig. 1.

The objective is to find the relation between a restoring force $\mathscr{F}$ and a deflection u. It is assumed that after a transient phase $[0, t_0]$, the pair $(u(t), \mathscr{F}(t))$ belongs to a periodic curve, called hysteresis loop (see Fig. 1 and Refs. [6,3]).

The MDM (see Section 2.1) and the MM with viscous damping (see Section 2.2) are used in the present investigation for modeling such behavior.

2.1. Theory of modified Dahl model

2.1.1. Modified Dahl model

Original Dahl model: In this paper, let $\dot{}$ be the derivative according to time t and Λ be a non-negative number. The Dahl model [3,11,12] is based on a differential equation expressing force $\mathscr{F}$ versus deflection u

$$\forall t \in [t_0, t_f], \quad \dot{\mathscr{F}}(t) + \Lambda \mathscr{F}(t)|\dot{u}(t)| = \Lambda \dot{u}(t), \tag{1a}$$

$$\mathscr{F}(t_0) = \mathscr{F}_0. \tag{1b}$$

It should be mentioned that when Λ tends to infinity the Dahl model corresponds to Coulomb's friction law.

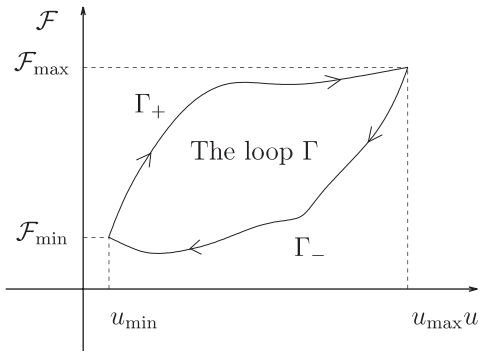

Fig. 1. The force-deflection loop Γ:Γ_+ is the increasing part and Γ_- is the decreasing part.

Duhem model: The Dahl model (1a) can be generalized by considering two functions h_u and h_l from $\mathbb{R}$ to $\mathbb{R}$ and the following differential equation, also known as the Duhem model (see Ref. [3]):

$$\forall t \in [t_0, t_f], \quad \dot{\mathscr{F}}(t) = \begin{cases} \Lambda \dot{u}(t)(h_u(u(t)) - \mathscr{F}(t)) & \text{if } \dot{u}(t) \geqslant 0, \\ -\Lambda \dot{u}(t)(h_l(u(t)) - \mathscr{F}(t)) & \text{if } \dot{u}(t) \leqslant 0. \end{cases} \tag{2}$$

Modified Dahl model: Generalizing Eq. (2) and introducing a parameter $\mu \in \mathbb{R}_+$ by the following relation:

$$\forall t \in [t_0, t_f], \quad \dot{\mathscr{F}}(t) = \begin{cases} \Lambda \dot{u}(t) \operatorname{sgn}(h_u(u(t)) - \mathscr{F}(t)) |h_u(u(t)) - \mathscr{F}(t)|^\mu & \text{if } \dot{u}(t) \geqslant 0, \\ -\Lambda \dot{u}(t) \operatorname{sgn}(h_l(u(t)) - \mathscr{F}(t)) |h_l(u(t)) - \mathscr{F}(t)|^\mu & \text{if } \dot{u}(t) \leqslant 0 \end{cases} \tag{3}$$

gives the MDM. Let a, b, d and e real numbers; it is assumed that for any $u \in \mathbb{R}$

$$h_u(u) = au + b, \quad h_l(u) = du + e. \tag{4}$$

The model governed by Eqs. (3) and (4) is presented and used in Refs. [6,7] or in Ref. [13].

2.1.2. Existence, uniqueness and regularity results for the MDM

According to the results of Refs. [6,11,12,14], differential Eq. (3) is a particular case of the Krasnosel'skiĭ–Pokrovskiĭ model: if u belongs to the Sobolev space of absolutely continuous functions $W^{1,1}(t_0, t_f)$, solution $\mathscr{F}$ of Eq. (3) with initial condition (1b) exists is unique and belongs to $W^{1,1}(t_0, t_f)$.

By using the notion of hysteresis operator (see for example Ref. [3]), let $\mathscr{C}_1$ be the operator which is associated to function u from $[t_0, t_f]$ to $\mathbb{R}$ and to number $\mathscr{F}_0$, the unique function $\mathscr{F}$ from $[t_0, t_f]$ to $\mathbb{R}$, satisfying (1b)–(3). $\mathscr{C}_1$ is an operator from $W^{1,1}(t_0, t_f) \times \mathbb{R}$ to $W^{1,1}(t_0, t_f)$ and (1b)–(3) is equivalent to (see [3, Chapter V]):

$$\forall t \in [t_0, t_f], \quad \mathscr{F}(t) = [\mathscr{C}_1(u, \mathscr{F}_0)](t). \tag{5}$$

2.1.3. Analysis of hysteresis and identification of parameters h_u, h_l, μ and Λ

Parameter Λ characterizes the transient velocity between h_u and h_l while exponent μ plays a predominant role in the loop shape.

Here, it is assumed that u and $\mathscr{F}$ are periodic. If $\mu = 1$, then the form of the hysteresis $(u, \mathscr{F})$ and the analytical expression of $\mathscr{F}$ permit estimating functions h_u and h_l and parameter Λ. Bliman in Refs. [11,12] showed that h_u and h_l are reached asymptotically: this property enables estimating h_u and h_l. Moreover, the comparison of the measured hysteresis loop area with the analytical one permits adjusting the value of Λ (with the method used in Ref. [13], for example).

For a general case, μ belongs to $\mathbb{R}_+$, as the analytical expression of $\mathscr{F}$ is not known and the identification of h_u, h_l, Λ and μ is not possible. However, h_u and h_l remain asymptotes of the hysteresis loop which makes their determination possible. The analytical determination of Λ and μ is not possible, but they are identified by successive comparisons between measured and predicted loops until satisfactory concordance is obtained (Fig. 2).

Differential Eqs. (1b)–(3) are solved by using a multi-step solver of Matlab, based on backward differentiation formulae (Gear's method).

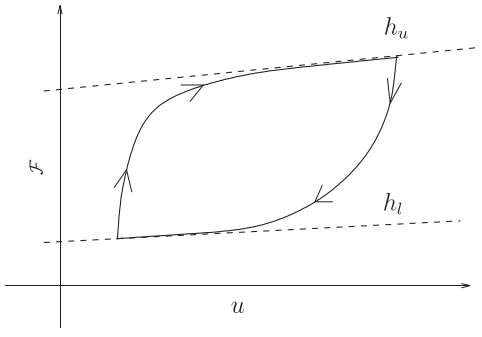

Fig. 2. The force-deflection loop Γ for the MDM.

2.2. Theory of the Masing model

Multi-valued friction models have been studied in Ref. [15] and in the survey [16]. Numerous works are founded on the Masing model (without damping) (see for example Ref. [5]). More elastoplastic models with finite numbers of degrees of freedom are presented in Refs. [17,4].

2.2.1. Description of the Masing model with viscous damping

The classical Masing model is often used in the case of elastoplastic behavior. It is composed of two springs and a dry friction element connected together, as shown in Fig. 3(a), where parameters k and k_0 are the stiffnesses of the two springs and α the threshold of the dry friction element. This association was studied for example in Ref. [4].

A viscous damping element c is added in the previous model, as shown in Fig. 3(b). Let u_s and u_t be the deflections of spring k and the dry friction element, f and f_0 the forces exerted by springs k and k_0, f_1 the force exerted by damping element c, and l and l_0 the spring-free lengths.

Consider the graph of the multi-valued operator σ defined by (see Fig. 4(a))

$$\sigma(x) = \begin{cases} -1 & \text{if } x<0, \\ 1 & \text{if } x>0, \\ [-1,1] & \text{if } x=0. \end{cases} \tag{6}$$

Considering its inverse graph β (see Fig. 4(b)), we obtain

$$\beta(x) = \begin{cases} \emptyset & \text{if } x \in (-\infty,-1)\cup(1,+\infty), \\ \{0\} & \text{if } x \in (-1,1), \\ \mathbb{R}_- & \text{if } x=-1, \\ \mathbb{R}_+ & \text{if } x=1. \end{cases} \tag{7}$$

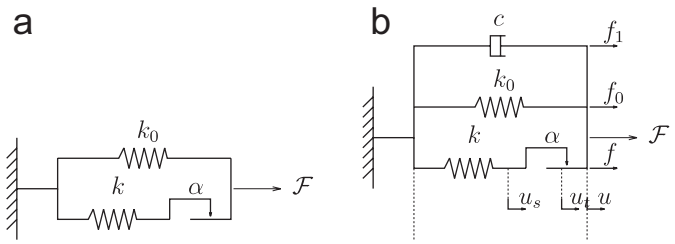

Fig. 3. The Masing model (a) with viscous damping (b).

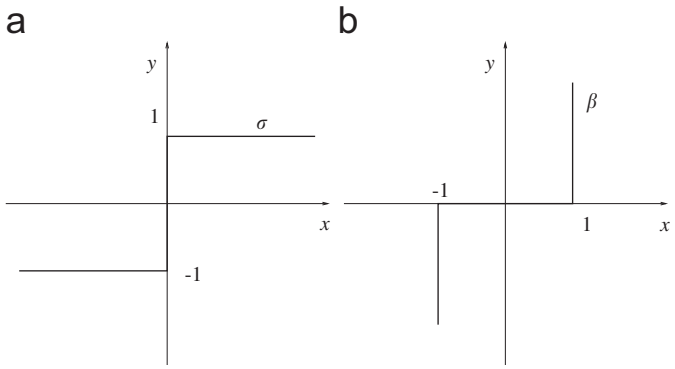

Fig. 4. The two used multi-valued maximal monotone graphs σ (a) and (b).

The graphs β and σ are maximal monotone (see for example Ref. [18]). The notion of sub-differential is recalled in Appendix A.1 (see Eqs. (A.4) and (A.6)). The maximal monotone graphs σ and β are sub-differentials of proper semi-continuous convex functions $|x|$ and $\psi_{[-1,1]}$ defined by

$$\forall x \in \mathbb{R}, \quad \psi_{[-1,1]}(x) = \begin{cases} 0 & \text{if } x \in [-1,1], \\ +\infty & \text{if } x \notin [-1,1]. \end{cases} \tag{8}$$

The constitutive law of the dry friction element is given by

$$f = \begin{cases} \tau \text{ with } \tau \in [-\alpha, \alpha] & \text{if } \dot{u}_t = 0, \\ -\alpha \operatorname{sgn}(\dot{u}_t) & \text{if } \dot{u}_t \neq 0. \end{cases} \tag{9}$$

Then, by using the multi-valued operator σ defined by Eq. (6), it is possible to write Eq. (9) in the form of the following differential inclusion: $f \in -\alpha\sigma(\dot{u}_t)$. By considering the constitutive laws of the springs, the dry friction element and the viscous damping element provide the following forces:

$$f_0 = -k_0(u - l_0), \tag{10a}$$

$$f = -k(u_s - l), \tag{10b}$$

$$f \in -\alpha\sigma(\dot{u}_t), \tag{10c}$$

$$f_1 = -c\dot{u}. \tag{10d}$$

The system equilibrium leads to

$$f + f_0 + f_1 + \mathscr{F} = 0 \tag{10e}$$

and the geometrical relation gives

$$u_s + u_t = u. \tag{10f}$$

By considering w, $\mathscr{F}_0$, η, defined by $w = u_s - l$, $\mathscr{F}_0 = k_0 l_0$, $\eta = \alpha/k$, $w_0 = w(t_0) \in [-\eta, \eta]$ and β defined by Eq. (7), it can be proved that system (10) is equivalent to

$$\dot{w} + \beta\left(\frac{w}{\eta}\right) \ni \dot{u}, \tag{11a}$$

$$w(t_0) = w_0, \tag{11b}$$

$$\mathscr{F} = kw + k_0 u + c\dot{u} - \mathscr{F}_0. \tag{11c}$$

2.2.2. Existence, uniqueness and regularity results for the Masing model with viscous damping

Proposition 1 of Appendix A.1 shows that the solution of Eqs. (11a)–(11b) exists and is unique. Thus, function $\mathscr{F}$ defined by Eq. (11c), exists and is unique.

By considering the notion of operator we prove that there exists an operator $\mathscr{C}_2$ from $H^2(t_0, t_f) \times [-\eta, \eta]$ to $W^{1,\infty}(t_0, t_f)$ such that Eq. (11) is equivalent to

$$\forall t \in [t_0, t_f], \quad \mathscr{F}(t) = [\mathscr{C}_2(u, w_0)](t). \tag{12}$$

Consequently, the MM and the MDM are both hysteresis operators.

2.2.3. Analysis of hysteresis

As in Ref. [4], it is assumed that function $\mathscr{F}$, defined by Eq. (11c), is also periodic; under this assumption, it is proved that the loop $(u, \mathscr{F})$ permits determining mechanical parameters of the MM with viscous damping.

Eq. (11c) can be rewritten as

$$\mathscr{F}_{\text{ep}}(t) = kw(t) + k_0 u(t) - \mathscr{F}_0, \tag{13a}$$

$$\mathscr{F}_v(t) = c\dot{u}(t), \tag{13b}$$

$$\mathscr{F}(t) = \mathscr{F}_{\mathrm{ep}}(t) + \mathscr{F}_{v}(t). \tag{13c}$$

The terms $\mathscr{F}_{\mathrm{ep}}$ and $\mathscr{F}_{v}$ correspond to the elastoplastic part and to the viscous part of the model, respectively.

It is now assumed that

$$u \text{ is } \tau\text{-periodic;} \tag{14a}$$

there exists τ_1, τ_2 and $\tau_3 = \tau_1 + \tau$, such that

$$u \text{ is strictly increasing on } [\tau_1, \tau_2] \text{ and strictly decreasing on } [\tau_2, \tau_3]; \tag{14b}$$

$$u \in C^2([t_0, t_f]); \tag{14c}$$

and setting

$$u_{\min} = \min(u), \quad u_{\max} = \max(u). \tag{14d}$$

If no damping is considered, then $\mathscr{F}_{v}$ is nil and we can prove under assumption (14a), as in Ref. [4], that the pair $(u, \mathscr{F})$ versus time plots a hysteresis loop. This loop represents a clockwise-oriented parallelogram as t is increasing on the interval $[t_0, t_f]$ (see Fig. 5). A direct correspondence exists between the six parallelogram parameters and the six system parameters $u_{\min}$, $u_{\max}$, k_0, k, α and $\mathscr{F}_0$, thus permitting their identification.

On the other hand, when damping is considered, the pair $(u, \mathscr{F})$ does not plot a hysteresis loop, in the classical sense of Ref. [3]. Indeed, the pair $(u, \mathscr{F}_{\mathrm{ep}})$ plots a hysteresis loop called the dry skeleton. However, since the second term $\mathscr{F}_{v}$ depends on the deflection history, the pair $(u, \mathscr{F}_{v})$ does not draw a hysteresis loop. Moreover, with $c \neq 0$, the identification of the mechanical parameters is still possible due to geometrical data of the loop.

The loop studied $(u(t), \mathscr{F}(t))$ for t belonging to $[t_0, t_f]$ is symmetric and only the upper half part of this curve is studied, as in Ref. [4]. In this last part $[\tau_1, \tau_2]$, u is strictly increasing and there is a bijection ψ_+ such that, for any $t \in [\tau_1, \tau_2]$, $t = \psi_+(u(t))$; moreover, $u(\tau_1) = u_{\min}$ and $u(\tau_2) = u_{\max}$. By considering $\mathscr{G}_+ = \dot{u} \circ \psi_+$, we obtain

$$\forall t \in [\tau_1, \tau_2], \quad \dot{u}(t) = \mathscr{G}_+(u(t)) \tag{15}$$

and Eq. (13) can be rewritten as

$$\forall u \in [u_{\min}, u_{\max}], \quad \mathscr{F}_{v}(u) = c\mathscr{G}_+(u), \tag{16}$$

and

$$\forall u \in [u_{\min}, u_{\max}], \quad \mathscr{F}(u) = \mathscr{F}_{\mathrm{ep}}(u) + \mathscr{F}_{v}(u), \tag{17}$$

where

$$\mathscr{F}_{\mathrm{ep}}(u) = kw(u) + k_0 u - \mathscr{F}_0, \tag{18}$$

where w depends only on u via the differential inclusion (11a).

If the deflection amplitude is large enough, then it exists $\tau_4 \in [\tau_1, \tau_2]$ so that

$$w(\tau_1) = -\eta, \quad w(\tau_4) = \eta. \tag{19}$$

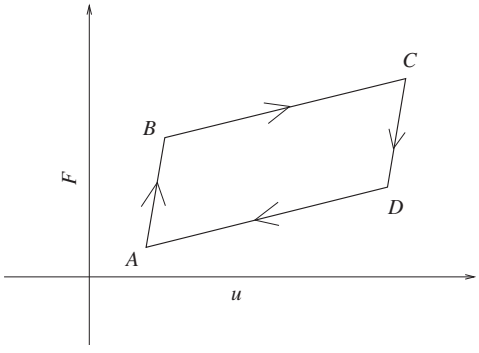

Fig. 5. The parallelogram loop for classical Masing model.

Henceforth, we consider

$$t_A = \tau_1, \quad t_B = \tau_4, \quad t_C = \tau_2, \tag{20a}$$

$$u_A = u(\tau_1), \quad u_B = u(\tau_4), \quad u_C = u(\tau_2), \tag{20b}$$

$$\mathscr{F}_A = \mathscr{F}(u_A), \quad \mathscr{F}_B = \mathscr{F}(u_B), \quad \mathscr{F}_C = \mathscr{F}(u_C). \tag{20c}$$

On the interval $[\tau_1, \tau_4]$, the dry friction element sticks and the model sketched in Fig. 3(b) is identical to the association of a spring with stiffness $k + k_0$ and a damping viscous element. After computation, thanks to Eq. (19), we obtain

$$\forall u \in [u_A, u_B], \quad \mathscr{F}(u) = (k + k_0)u - \mathscr{F}_0 - k(u_A + \eta) + c\mathscr{G}_+(u). \tag{21a}$$

On the contrary, on the interval $[\tau_4, \tau_2]$, the dry friction element slips and the model sketched in Fig. 3(b) is identical to the association of a spring with stiffness k_0 and a damping viscous element. After computation, we obtain

$$\forall u \in [u_B, u_C], \quad \mathscr{F}(u) = k_0 u + k\eta - \mathscr{F}_0 + c\mathscr{G}_+(u). \tag{21b}$$

By using Eqs. (21), the shape of the loop $(u, \mathscr{F})$ is given in Fig. 6, where the dry skeleton corresponds to the pair $(u, \mathscr{F}_{ep})$. Corners A and C represent slip–stick state change whereas the corners B and D represent stick–slip state change.

2.2.4. *Parameter identification*

We proved in previous section that the mechanical characteristic of the model gives the shape of the hysteresis. Reciprocally, we now prove that we identify model parameters can be identified from the experimental hysteresis loop.

For $u = u_A$, $\dot{u}$ is equal to zero and then $\mathscr{G}_+(u_A)$ is equal to zero; thus, Eq. (21) gives

$$\mathscr{F}_A = (k + k_0)u_A - \mathscr{F}_0 - k(u_A + \eta) \tag{22a}$$

and

$$\mathscr{F}_C = k_0 u_C + k\eta - \mathscr{F}_0. \tag{22b}$$

With Eq. (21a), for $u = u_A$ and $u = u_B$, we obtain

$$u_B - u_A = 2\eta. \tag{22c}$$

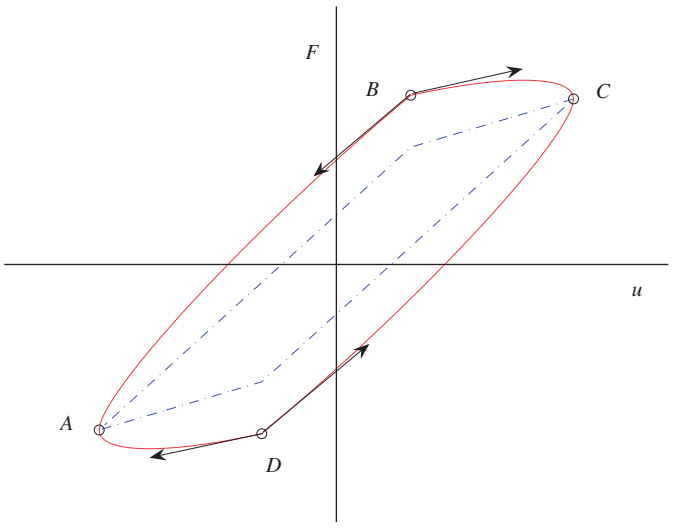

Fig. 6. The force-deflection loop Γ for the MM with viscous damping (solid line), the dry skeleton (dot-dashed line).

By definition,

$$u_A = u_{\min}, \quad u_C = u_{\max}. \tag{22d}$$

Let p_B^+ and p_B^- be the right and left derivatives of $\mathscr{F}$ according to u at point u_B; According to Eqs. (21) and since u is of class C^1:

$$p_B^+ = k_0 + c\mathscr{G}'_+(u_B), \tag{23a}$$

$$p_B^- = k + k_0 + c\mathscr{G}'_+(u_B). \tag{23b}$$

Thanks to assumption (14c), $\mathscr{G}'_+$ is continuous in u_B and we obtain

$$p_B^- - p_B^+ = k. \tag{24}$$

Moreover, point B is the unique point of the upper part of the loop $(u, \mathscr{F})$ where the derivative is not continuous.

Similarly, on the decreasing part of the loop, the same approach is developed. We consider, if u is strictly decreasing, $t = \psi_-(u(t))$ and we obtain

$$\forall u \in [u_D, u_C], \quad \mathscr{F}(u) = (k + k_0)u - \mathscr{F}_0 - k(u_C - \eta) - c\mathscr{G}_-(u), \tag{25a}$$

$$\forall u \in [u_A, u_D], \quad \mathscr{F}(u) = k_0 u - k\eta - \mathscr{F}_0 - c\mathscr{G}_-(u). \tag{25b}$$

As in Ref. [4], the following equations remain true and permit parameter identification:

$$u_{\min} = u_A, \tag{26a}$$

$$u_{\max} = u_C, \tag{26b}$$

$$k = p_B^- - p_B^+, \tag{26c}$$

$$\alpha = \frac{k}{2}(u_B - u_A), \tag{26d}$$

$$k_0 = \frac{\mathscr{F}_C - \mathscr{F}_A - 2\alpha}{u_C - u_A}, \tag{26e}$$

$$\mathscr{F}_0 = k_0 u_A - \alpha - \mathscr{F}_A. \tag{26f}$$

These equations are obtained by Eqs. (22) and (24).

However, the value of c must be determined. A similar method to that of Ref. [13] is used to estimate the value of Λ for $\mu = 1$. By equaling the calculated and measured energies dissipated by the viscous damping element, i.e. the inside area of the loops $(u, c\dot{u})$, we can write Eq. (13) as

$$\mathscr{F} - (kw + k_0 u - \mathscr{F}_0) = \mathscr{F} - \mathscr{F}_{\text{ep}} = \mathscr{F}_v = c\dot{u} = c\mathscr{G}_+,$$

or thanks to Eqs. (21) and (25)

$$\forall u \in [u_A, u_B], \quad \mathscr{F}(u) - ((k + k_0)u - \mathscr{F}_0 - k(u_A + \eta)) = c\mathscr{G}_+(u), \tag{27a}$$

$$\forall u \in [u_B, u_C], \quad \mathscr{F}(u) - (k_0 u + k\eta - \mathscr{F}_0) = c\mathscr{G}_+(u), \tag{27b}$$

$$\forall u \in [u_D, u_C], \quad \mathscr{F}(u) - ((k + k_0)u - \mathscr{F}_0 - k(u_C - \eta)) = -c\mathscr{G}_-(u), \tag{27c}$$

$$\forall u \in [u_A, u_D], \quad \mathscr{F}(u) - (k_0 u - k\eta - \mathscr{F}_0) = -c\mathscr{G}_-(u). \tag{27d}$$

The loop $(u, c\dot{u})$ is an elliptic curve. The two functions $\mathscr{G}_+$ and $\mathscr{G}_-$ are known and the energy dissipated $\mathscr{E}$ has the following expression:

$$\mathscr{E} = c\int_{u_{\min}}^{u_{\max}} \mathscr{G}_+(u) - \mathscr{G}_-(u)\,\mathrm{d}u = c\left(\int_{\substack{t_A \\ u \text{ increasing}}}^{t_C} \dot{u}^2(t)\,\mathrm{d}t - \int_{\substack{t_C \\ u \text{ decreasing}}}^{t_A} \dot{u}^2(t)\,\mathrm{d}t\right). \tag{28}$$

If u is defined by

$$\forall t, \quad u(t) = x_0 + x_1 \sin(\Omega t + \phi), \tag{29}$$

Eq. (28) yields

$$\mathscr{E} = \pi x_1^2 \Omega c. \tag{30}$$

The value of damping c is determined for pulsation Ω. In Section 4, the pulsation Ω is different and equal to Ω_0. Hence, it assumed that the product $c\Omega$ is constant, which permits using value c_0:

$$c_0 = \frac{\Omega}{\Omega_0} c, \tag{31}$$

where c is given by Eq. (30).

This assumption is based on the experiments performed in Ref. [13] and is confirmed by the calculations presented in Section 4. Eqs. (11a) and (11b) have analytical solutions in specific cases as for u defined by Eq. (29). Consequently, function $\mathscr{F}$ is determined by Eq. (11c).

3. Experimental investigation and parameter identification

The tensioner is composed of three parts, see Fig. 7 (a): Part 1 is a solid (Idler pulley) that rotates around axis $\Delta = (AB)$ of part 2; part 2 is the tensioner arm ABC, that rotates around the fixed axis Δ' of part 3, bolted to the reference part 4 (i.e. an engine for automotive applications). All the parts are considered as rigid bodies. The pin joint of axis Δ' between parts 2 and 3 includes a torsion spring and friction components that cause dry and lubricated contact forces, and a moment between parts 2 and 3. The phenomena involved result in highly nonlinear behavior of the joint.

An experimental setup has been designed for identifying the belt tensioner model parameters. The idler pulley is removed and segment AB is connected to a rigid bar that subjects a vertical alternative displacement on point A. The vertical displacement $u(t)$ of point A, and of force $\mathscr{F}$ are considered positive when oriented toward the ground, since in use, the tensioner is always preloaded. Force $\mathscr{F}$ remains positive.

The displacements are measured using laser optical sensors, while the forces are measured with load cells. Data acquisition is performed simultaneously with a sample frequency $f_{\text{sto}} = 5000\,\text{Hz}$. The measurements can be filtered to remove measurement noise.

3.1. Experimental setup for identifying the parameters of the models

An alternative vertical displacement is imposed on point A, defined by Eq. (29), with

$$\Omega = 9.4\,\text{rad/s}, \quad \phi = 4.8\,\text{rad}, \quad x_0 = 5.4 \times 10^{-4}\,\text{m}, \quad x_1 = 5.2 \times 10^{-4}\,\text{m}. \tag{32}$$

After a transient state (start from initial position), a steady hysteretic loop is observed as shown in Fig. 8 and the measured force $\mathscr{F}$ versus time is periodic.

If u and $\mathscr{F}$ are measured in the case of a larger imposed displacement amplitude, then a hysteresis loop as shown like in Ref. [13] is observed. Compared to the loop of Fig. 8, the $\max(u) - \min(u)$ range of deflection is larger. In Ref. [13], the authors have shown that the MDM parameters are dependent on x_0 and to a lesser extent on Ω. This dependency is not considered here: the values of x_0 and x_1, given by Eq. (32), have been chosen so that the $\max(u) - \min(u)$ range, observed in Fig. 8 should be similar to that observed in Section 4. Moreover, it is supposed that the characteristics of the models studied depend on the $\max(u) - \min(u)$ range but do not depend on forcing frequency Ω.

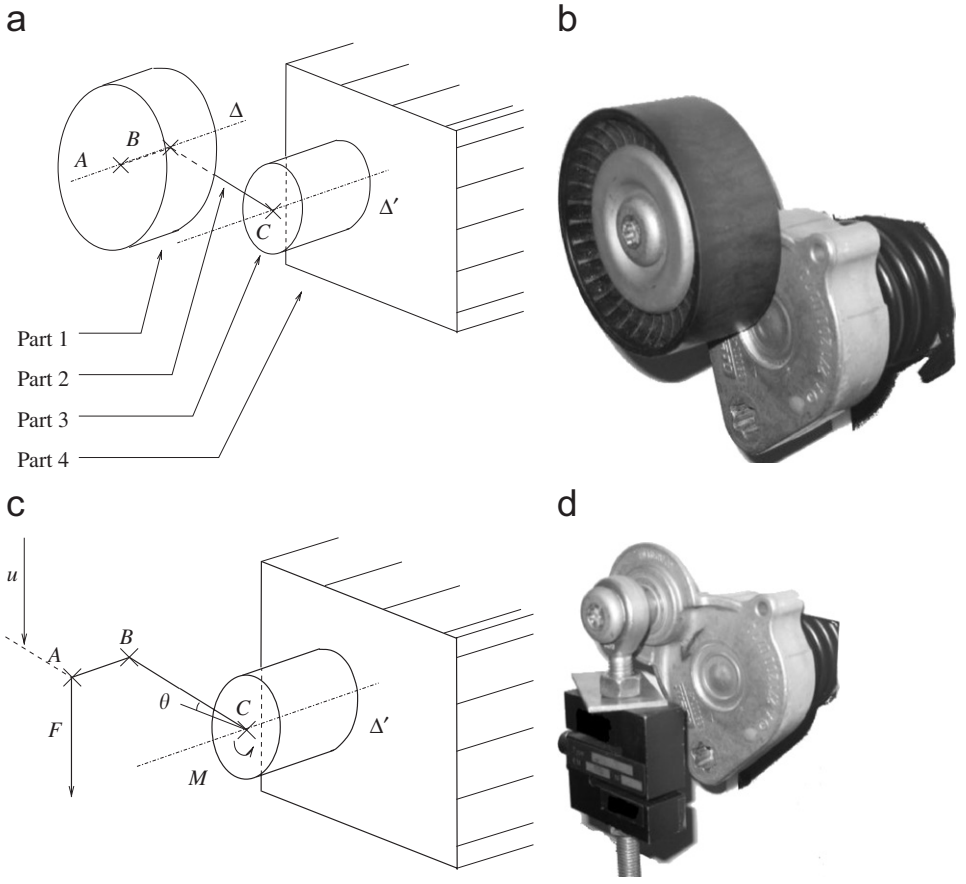

Fig. 7. Tensioner schemes and pictures: complete (a,b) and without pulley (c,d).

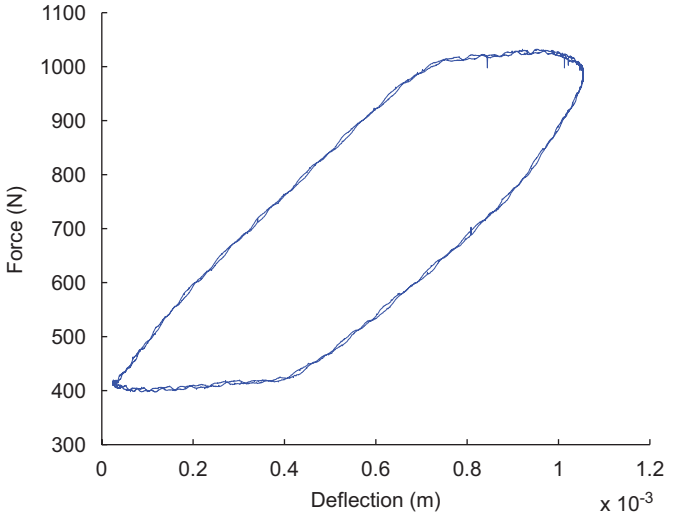

Fig. 8. Measured loop $(u, \mathscr{F})$.

3.2. Identification of the model parameters

3.2.1. Modified Dahl model

In order to identify the parameters defining h_u and h_l, the method of Section 2.1.3 is used: as in Ref. [13], h_u and h_l represent the upper and lower envelop curves of the hysteretic loop Γ to which the pair $(u(t), \mathscr{F}(t))$ belongs when t describes $[t_0, t_f]$. For the next development it is considered that u is defined by Eqs. (29) and (32).

From the analysis of the measured loop represented in Fig. 8, the envelop curves h_u and h_l can be considered as straight lines and therefore the values of a, b, d and e are determined using the mean squares approximation method (see Fig. 9):

$$a = 7.146 \times 10^4\,\mathrm{N/m}, \quad b = 9.596 \times 10^2\,\mathrm{N}, \quad d = 5.322 \times 10^4\,\mathrm{N/m}, \quad e = 3.972 \times 10^2\,\mathrm{N}. \tag{33}$$

In order to use the MDM, the initial condition $(t_0, \mathscr{F}_0)$ is chosen such that t_0 corresponds to an arbitrary point of the u–$\mathscr{F}$ loop, ensured to be after the transient phase:

$$t_0 = 1.988 \times 10^{-1}\,\mathrm{s}, \quad \mathscr{F}_0 = 1.009 \times 10^3\,\mathrm{N}. \tag{34}$$

Moreover, using the results of Section 2.1.3 and after several numerical iterations, the optimal values of parameters Λ and μ are determined:

$$\Lambda = 117355, \quad \mu = 0.37. \tag{35}$$

3.2.2. Masing model with viscous damping

In order to identify the parameters of the MM with viscous damping, i.e. $\{u_{\min}, u_{\max}, k, k_0, \alpha, \mathscr{F}_0, c\}$, the results of Section 2.2.4 are applied to the experimental loop represented in Fig. 8.

As shown in Fig. 10, the numerical values of u_A, u_B, u_C, $\mathscr{F}_A$, $\mathscr{F}_C$, p_B^-, and p_B^+ are determined, and thanks to Eqs. (26) and (30) we obtain the following data:

$$u_{\min} = 2 \times 10^{-5}\,\mathrm{m}, \quad u_{\max} = 1.05 \times 10^{-3}\,\mathrm{m}, \tag{36a}$$

$$k = 4.84 \times 10^5\,\mathrm{N/m}, \quad k_0 = 2.34 \times 10^5\,\mathrm{N/m}, \quad \alpha = 1.63 \times 10^2\,\mathrm{N}, \quad \mathscr{F}_0 = -5.73 \times 10^2\,\mathrm{N}. \tag{36b}$$

$$c = 1.93 \times 10^4\,\mathrm{N\,s/m}. \tag{36c}$$

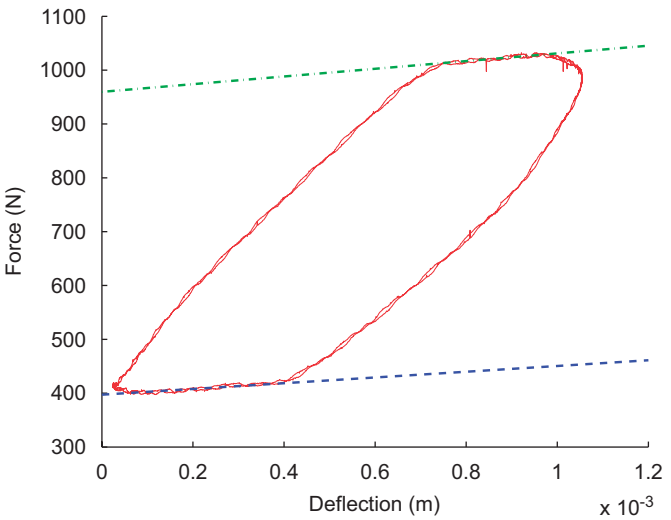

Fig. 9. Identification of the envelop curves h_u (dot-dashed line) and h_l (dashed line), measured loop (solid line).

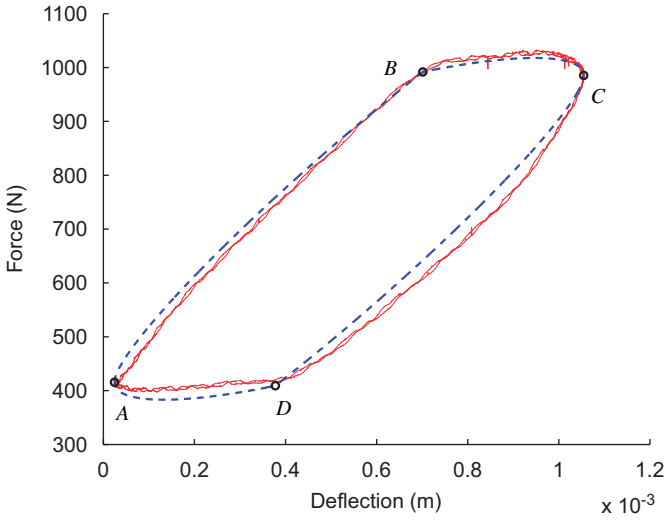

Fig. 10. Predicted (MM with viscous damping, dashed line) and measured (solid line).

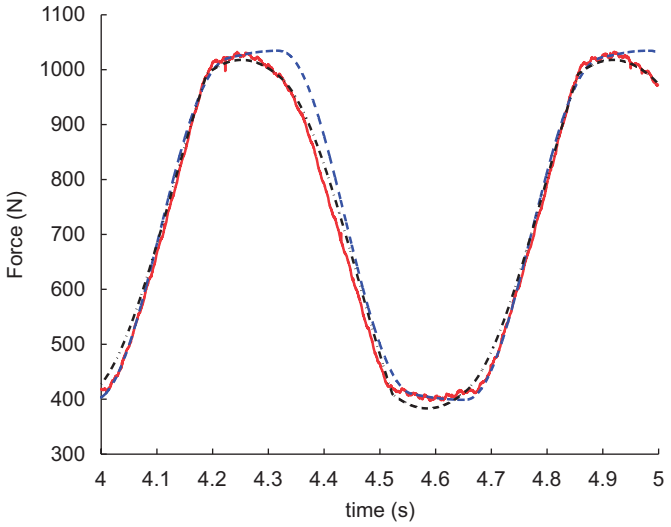

Fig. 11. Identification part: the force $\mathscr{F}$ versus time measured (solid line) and predicted with the MDM (dashed line) and with the MM (dot-dashed line).

As in Section 3.2.1, the initial condition $(t_0, w_0 = w(t_0))$ is chosen such that t_0 corresponds to an arbitrary point of the u–$\mathscr{F}$ loop, ensured to be after the transient phase:

$$t_0 = 1.55 \times 10^{-2}\,\mathrm{s}, \quad w(t_0) = -3.24 \times 10^{-4}\,\mathrm{m}. \tag{37}$$

3.3. Comparison of the results obtained with the modified Dahl and Masing models and with the experiment

The previous identification permits predicting the force for an imposed deflection; numerical and analytical computations were performed for the MDM and the MM. The curves $t \mapsto \mathscr{F}$ are plotted in Fig. 11. Since the curves obtained are periodic, not all the periods are shown.

The force-deflection loop $u \mapsto \mathscr{F}$ is plotted in Fig. 12. By comparing the force-deflection loops, it appears that the stick–slip state transition is modeled differently. Indeed, for the MDM (Fig. 12(a)), the slope of the

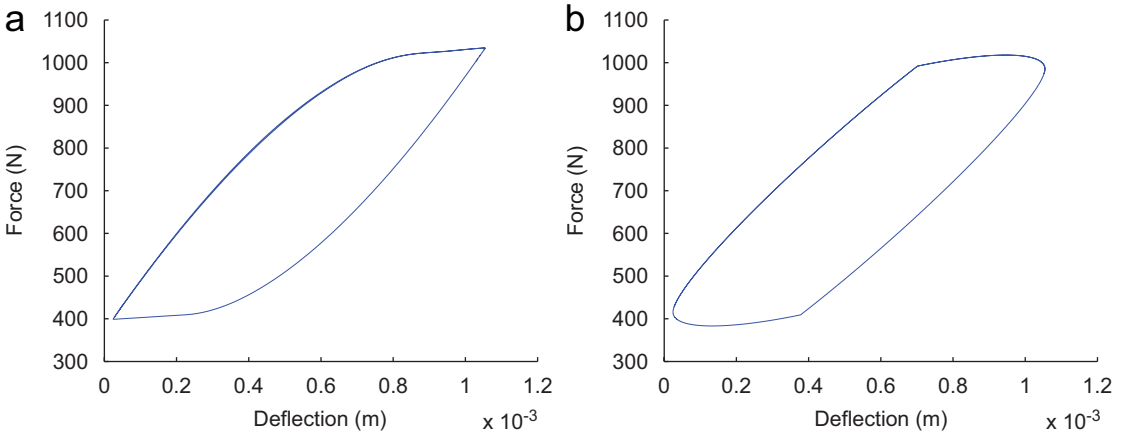

Fig. 12. Identification part: the predicted load $\mathscr{F}$ versus deflection u with the MDM (a) and with the MM (b).

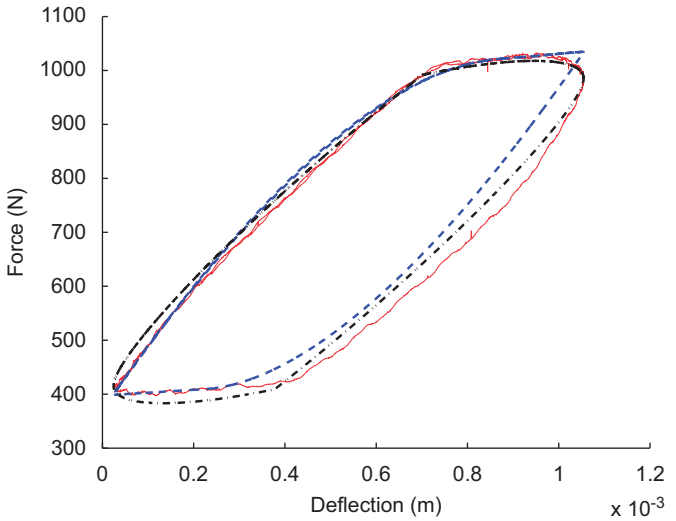

Fig. 13. Identification part: load $\mathscr{F}$ versus deflection u measured (solid line) and predicted with the MDM (dashed line) and with the MM (dot-dashed line).

force versus deflection curve at the stick–slip transition is continuous though it is not for the slip–stick transition. This is the contrary for the MM with viscous damping (Fig. 12(b)). In addition, the higher the viscous damping, the smoother the slip–stick transition will be.

Both experimental and numerical results are presented in Figs. 11 and 13. Good agreement can be observed between the two theoretical models and also between each model and the experiment performed to validate the models used and their identification.

4. Comparison, validation and prediction

In the previous section, the MDM and MM were formulated for the belt tensioner. The tensioner is now a part of a mechanical system subjected to a variable load excitation. The purpose is to test the models efficiency considering a multi-degree of freedom system and an experimental investigation. Each tensioner model is implemented in the system motion equations that are solved numerically. The predicted and measured results are compared.

4.1. Equations of motion for the system

4.1.1. System description

The dynamic system considered is composed of the previously studied tensioner, a poly-V belt and a mass (see Fig. 14). The tensioner base is fixed on a rigid frame. Its idler pulley of mass m_2 has a belt wrapped around it. The two adjacent belt spans are joined at their other end and connected to a mass m_1. The mass m_1 is excited by the imposed force f generated by an electro-dynamic shaker (see Fig. 14). Two displacements u_1 and u_2 (see Fig. 15) of the two masses are measured with laser–optical displacement sensors. The transmitted force

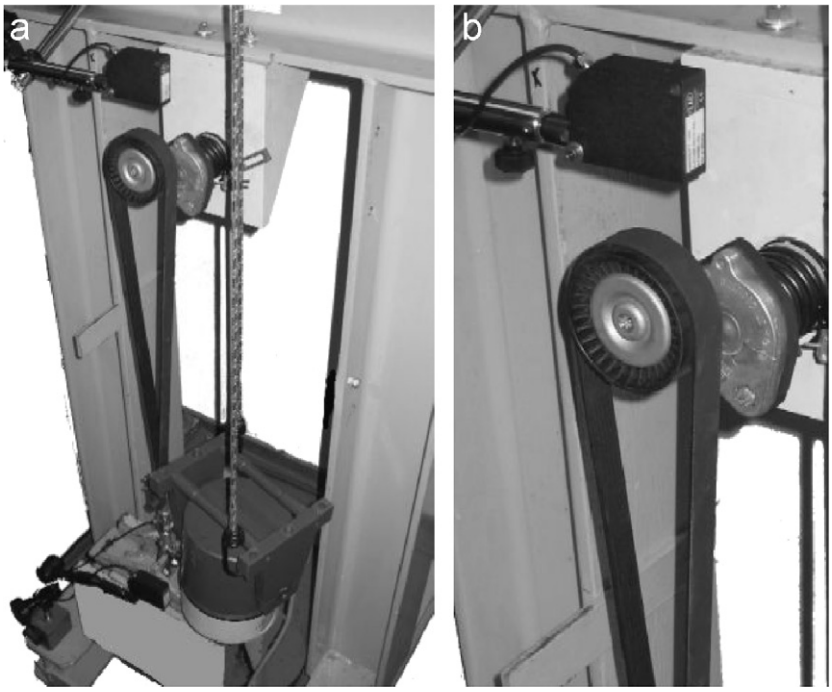

Fig. 14. Experimental setup: belt–tensioner–mass system; total system (a) and zoom (b).

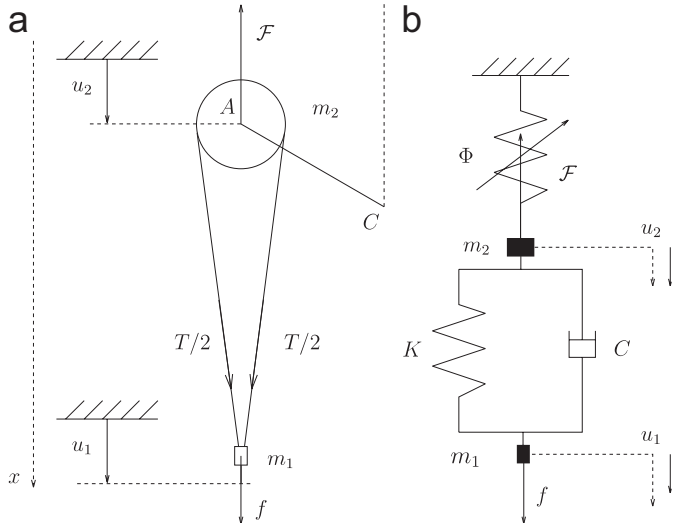

Fig. 15. Sketch (a) and model (b) of belt–tensioner–mass system.

f is measured with a piezo-electric load sensor, and the belt tension is measured with an S-shape load sensor. In this two degrees of freedom system, mass m_1 is used both for the tensioner preload and for the system dynamics.

4.1.2. System equations

Let u_1 and u_2 be the vertical displacements of masses 1 and 2, along the x axis, both positive oriented downward. As in Section 3, $\mathscr{F}$ is the force exerted by the tensioner, it is positive oriented upward. Force f is positive oriented downward (see Fig. 15). Let $T/2$ be the tension in each belt span. Due to the ratio between the radius of the pulley and the belt span lengths, it is assumed that tension T is oriented vertically.

The gravity constant is noted as g and equations governing the complete system are given by

- The belt behavior law, by considering the belt as a spring-damper of stiffness K and equivalent viscous damping C:

$$T(t) = K(u_1(t) - u_2(t)) + C(\dot{u}_1(t) - \dot{u}_2(t)) + \mathscr{T}_0, \tag{38a}$$

  where $\mathscr{T}_0$ is related to the initial belt tension.
- The dynamic equilibrium of the tensioner pulley projected along the vertical axis x, by neglecting effects on the horizontal axis:

$$m_2\ddot{u}_2(t) = T(t) - \mathscr{F}(t) + m_2 g. \tag{38b}$$

- The dynamic equilibrium of the lower mass projected along the vertical axis x, by neglecting effects on the horizontal axis:

$$m_1\ddot{u}_1(t) = -T(t) + f(t) + m_1 g. \tag{38c}$$

- Initial data at t_0 for u_1 and u_2:

$$u_1(t_0) = u_{1,0}, \quad \dot{u}_1(t_0) = \dot{u}_{1,0}, \quad u_2(t_0) = u_{2,0}, \quad \dot{u}_2(t_0) = \dot{u}_{2,0}. \tag{38d}$$

- The relation between force $\mathscr{F}$ and displacement u_2 is written formally as

$$\mathscr{F} = \Phi(u_2), \tag{38e}$$

  where Φ is an operator.

Belt stiffness K and damping C are obtained by using an experimental model analysis non-presented here. The parameter values of the system are fixed:

$$m_1 = 73.84\,\text{kg}, \quad m_2 = 0.15\,\text{kg}, \quad K = 560\,000\,\text{N/m}, \quad C = 160\,\text{N s/m}, \quad g = 9.81\,\text{m/s}^2. \tag{39}$$

The initial conditions are chosen arbitrarily

$$u_{1,0} = 0, \quad \dot{u}_{1,0} = 0, \quad u_{2,0} = 0, \quad \dot{u}_{2,0} = 0, \tag{40a}$$

and t_0 corresponds to an arbitrary point of the u–$\mathscr{F}$ loop, ensured to be after the transient phase:

$$t_0 = 1.6 \times 10^{-3}\text{s}. \tag{40b}$$

4.1.3. Application of the modified Dahl model

Applying the MDM for the tensioner implemented in the system, consists in replacing u by u_2 in Eqs. (1b)–(3):

$$\dot{\mathscr{F}}(t)) = \begin{cases} \Lambda\dot{u}_2(t)\,\text{sign}(h_u(u_2(t)) - \mathscr{F}(t))\,|h_u(u_2(t)) - \mathscr{F}(t)|^{\mu} & \text{if } \dot{u}_2(t) \geqslant 0, \\ -\Lambda\dot{u}_2(t)\,\text{sign}(h_l(u_2(t)) - \mathscr{F}(t))\,|h_l(u_2(t)) - \mathscr{F}(t)|^{\mu} & \text{if } \dot{u}_2(t) \leqslant 0, \end{cases} \tag{41}$$

$$\mathscr{F}(t_0) = \mathscr{F}_0. \tag{42}$$

Finally, it is necessary to solve the system formed by Eqs. (38a), (38b), (38c), (41) and initial conditions (38d) and (42). It is admitted that u_1, u_2, T and $\mathscr{F}$ exist and are unique.

4.1.4. Application of the Masing model with viscous damping

For the MM with viscous damping, replacing u by u_2 transforms Eq. (11) in

$$\dot{w} + \beta\left(\frac{w}{\eta}\right) \ni \dot{u}_2 \quad \text{on } [t_0, t_f], \tag{43a}$$

$$w(t_0) = w_0, \tag{43b}$$

$$\mathscr{F} = kw + k_0 u_2 + c\dot{u}_2 - \mathscr{F}_0 \quad \text{on } [t_0, t_f]. \tag{43c}$$

Finally, we obtain the system of Eqs. (38a), (38b), (38c), (43a), (43c), and initial conditions (38d) and (43b). These equations are written as a differential inclusion of the first order studied in Refs. [4,18]: we now consider $H = \mathbb{R}^5$, $\eta > 0$, and $Q = \mathbb{R}^4 \times [-\eta, \eta]$ a closed bounded interval of $\mathbb{R}$, the maximal monotone graph A is defined by

$$\forall X = (u_1, v_1, u_2, v_2, w) \in Q, \quad A(X) = \{0\} \times \{0\} \times \{0\} \times \{0\} \times \beta\left(\frac{w}{\eta}\right), \tag{44}$$

where β is defined by Eq. (7). Note that $A = \partial\psi_K$. Let K, C, $\mathscr{T}_0$, $\mathscr{F}_0$, c, k, k_0 and g, be numbers and m_1, m_2 be two non-negative numbers, function $\mathscr{H}$ from $[t_0, t_f] \times \mathbb{R}^5$ to $\mathbb{R}^5$ is defined by: for any $(t, X) = (t, u_1, v_1, u_2, v_2, w) \in [t_0, t_f] \times \mathbb{R}^5$

$$\mathscr{H}(t, X) = \begin{pmatrix} v_1 \\ \frac{1}{m_1}(-T + f(t)) + g \\ v_2 \\ \frac{1}{m_2}(-\mathscr{F} + T) + g \\ v_2 \end{pmatrix}, \tag{45a}$$

where

$$T = K(u_1 - u_2) + C(v_1 - v_2) + \mathscr{T}_0, \tag{45b}$$

$$\mathscr{F} = kw + k_0 u_2 + cv_2 - \mathscr{F}_0. \tag{45c}$$

For $(u_{1,0}, \dot{u}_{1,0}, u_{2,0}, \dot{u}_{2,0}, w_0) \in Q$, we consider

$$X_0 = \begin{pmatrix} u_{1,0} \\ \dot{u}_{1,0} \\ u_{2,0} \\ \dot{u}_{2,0} \\ w_0 \end{pmatrix}. \tag{46}$$

Let f be a function belonging to $H^1(t_0, t_f)$. By using Proposition 1 of Appendix A, there exists a unique solution $X \in W^{1,\infty}((t_0, t_f); \mathbb{R}^5)$ of

$$\dot{X}(t) + A(X(t)) \ni \mathscr{H}(t, X(t)) \quad \text{a.e. on } (t_0, t_f), \tag{47a}$$

$$X(t_0) = u_0, \tag{47b}$$

which is equivalent to (38a), (38b), (38c), (43a), (43c), and initial conditions (38d) and (43b).

4.2. The numerical scheme used and numerical simulations

4.2.1. Modified Dahl model

In order to solve numerically the differential system formed by Eqs. (38a), (38b), (38c) and (41), it is written in the form of a first-order equation. Function G from $\mathbb{R}^3$ to $\mathbb{R}$ is introduced and defined by

$$\forall(u,v,\mathscr{F})\in\mathbb{R}^3,\quad G(u,v,\mathscr{F})=\begin{cases}\Lambda v\,\mathrm{sign}(h_u(u)-\mathscr{F})\,|h_u(u)-\mathscr{F}|^{\mu} & \text{if } v\geqslant 0,\\ -\Lambda v\,\mathrm{sign}(h_l(u)-\mathscr{F})\,|h_l(u)-\mathscr{F}|^{\mu} & \text{if } v\leqslant 0,\end{cases}\tag{48}$$

with functions h_u and h_l defined by Eq. (4). Then Eq. (41) is equivalent to

$$\dot{\mathscr{F}}(t)=G(u_2(t),\dot{u}_2(t),\mathscr{F}(t)).$$

Let $\mathscr{G}$ be the function from $[t_0,t_f]\times\mathbb{R}^5$ to $\mathbb{R}^5$ defined by: for any $(t,X)=(t,u_1,v_1,u_2,v_2,\mathscr{F})\in[t_0,t_f]\times\mathbb{R}^5$

$$\mathscr{G}(t,X)=\begin{pmatrix} v_1\\ \dfrac{1}{m_1}(-T+f(t))+g\\ v_2\\ \dfrac{1}{m_2}(-\mathscr{F}+T)+g\\ G(u_2,v_2,\mathscr{F})\end{pmatrix},\tag{49a}$$

where

$$T=K(u_1-u_2)+C(v_1-v_2)+\mathscr{T}_0.\tag{49b}$$

By considering $X(t)=(u_1(t),\dot{u}_1(t),u_2(t),\dot{u}_2(t),\mathscr{F}(t))$ and $X_0=(u_{1,0},\dot{u}_{1,0},u_{2,0},\dot{u}_{2,0},\mathscr{F}_0)$, Eqs. (38a), (38b), (38c) and (41) with initial conditions (38d) and (42) are equivalent to

$$\forall t\in[t_0,T],\quad \dot{X}(t)=\mathscr{G}(t,X(t))\tag{50a}$$

with the initial condition

$$X(t_0)=X_0.\tag{50b}$$

Then T is deduced from Eq. (38a). To define $\mathscr{F}_0$ and $\mathscr{T}_0$, it is assumed that the system of Eqs. (38a), (38b), (38c) and (41) is still valid for the static equilibrium of the system, where u_1 and u_2 are nil at $t=t_0$:

$$\mathscr{F}(t_0)=f(t_0)+(m_1+m_2)g,\tag{51a}$$

$$\mathscr{T}_0=f(t_0)+m_1g.\tag{51b}$$

It is assumed that

$$f(t)=f_0+f_1\cos(\Omega_0 t+\phi),\tag{52}$$

with

$$f_0=3.5\,\mathrm{N},\quad f_1=122.1\,\mathrm{N},\quad \Omega_0=73.15\,\mathrm{rad/s},\quad \phi=0.40\,\mathrm{rad}.\tag{53}$$

The excitation force amplitude f_1 was chosen so that the $\max(u_2)-\min(u_2)$ displacement range is similar in magnitude to that of the parameter identification test (see Fig. 8). Therefore, the identified values of parameters a, b, d, e, Λ and μ can be used.

To solve the differential Eqs. (50), a numerical multi-step solver of Matlab, based on backward differentiation formulae (Gear's method), is used. It is admitted that the scheme is convergent.

The values chosen for $u_{1,0}$, $\dot{u}_{1,0}$, $u_{2,0}$, and $\dot{u}_{2,0}$, have little influence on the solution in periodic steady state. The results are presented in Section 4.3.

4.2.2. The Masing model with viscous damping

By using numerical scheme (A.9) applied to differential inclusion (47), it is possible to numerically calculate u_1, $\dot{u}_1$, $\ddot{u}_1$, u_2, $\dot{u}_2$, $\ddot{u}_2$, w, T and $\mathscr{F}$ at time t_p.

The numerical scheme is a discrete formulation of the motion equations. Using an implicit Euler scheme produces a first-order error whereas higher-order schemes seem to be better adapted (as Runge–Kutta 4). However, as a counter example, it has been shown in Ref. [17] that even when using more accurate schemes, the error remains of first order. Fundamentally, the presence of the multi-valued term A in (A.3) can lead to a discontinuous derivative of u and limits the order of the scheme to one.

Another method can be to use a different type of discretization based on the differentiation of the states in which the tensioner is stuck or slips. In each of the two states an ordinary differential equation has to be solved. This method has three main difficulties: firstly, it implies the determination of instant of change of state that can require long calculation times; secondly, nothing guarantees this is a first-order method, which can lead to inconsistent results in the case of large number of changes of state. Finally, the model developed here has only one dry friction element; the numerical scheme used remains the same in the case of several elements, and it can be easily generalized without many additional calculations. Solving the system separating the different states is difficult to manage.

It is assumed that f is defined by Eqs. (52) and (53). The initial conditions defined in Section 4.1.2 are used with an additional one:

$$w_0 = 0. \tag{54}$$

As with the MDM, Eq. (51) is used and gives

$$\mathscr{T}_0 = 338\,\mathrm{N}. \tag{55}$$

The values chosen for t_0, $u_{1,0}$, $\dot{u}_{1,0}$, $u_{2,0}$, $\dot{u}_{2,0}$, and w_0 have little influence on the solution in periodic steady state. The values of $u_{\min}$, $u_{\max}$, k, k_0, α and $\mathscr{F}_0$ identified can be used. For the value of c_0, Eq. (31) is used, where c is numerically supplied by Eq. (36c), Ω is defined by Eq. (32), and $\Omega_0 = \Omega$, defined by Eq. (53). We obtain

$$c_0 = 2.48 \times 10^3\,\mathrm{N\,s/m}. \tag{56}$$

For the MM with viscous damping, a numerical Euler implicit scheme of step h defined by

$$h = 10^{-5}\,\mathrm{s} \tag{57}$$

is used. The results are presented in the next section.

4.3. Predicted and measured responses

In this section, the predicted and measured responses of the multi-degrees of freedom system are presented and compared (see Fig. 16). No transient phase is observed for the measured responses.

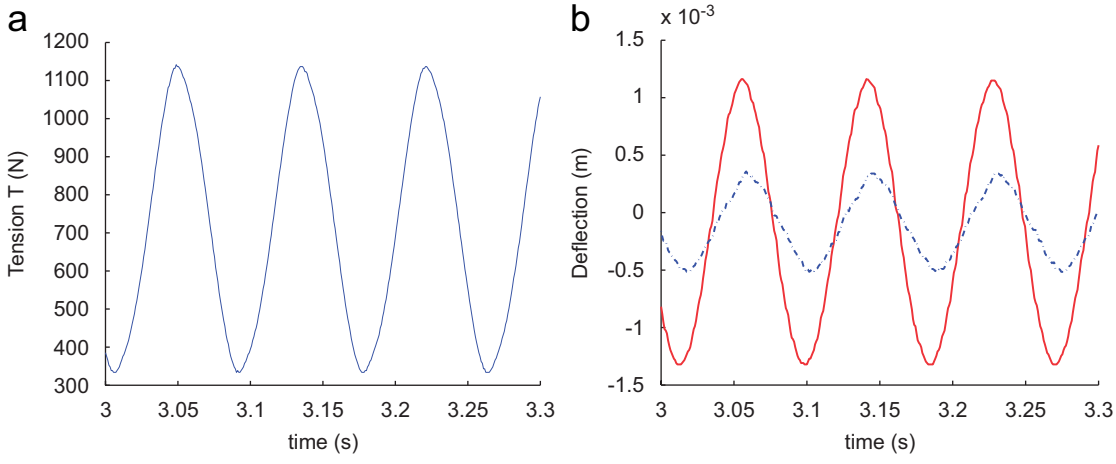

Fig. 16. Measured curves T (a), u_1 (b, solid line) and u_2 (b, dot-dashed line) versus time (on time interval $[3, 3.3]$).

The value of force $\mathscr{F}$ is reached using Eq. (38b) which gives

$$T(t) - \mathscr{F}(t) = m_2(\ddot{u}_2(t) - g)$$

and since m_2 defined by Eq. (39) is negligible compared to m_1, it leads to

$$T(t) \approx \mathscr{F}(t). \tag{58}$$

To confirm this assumption, $\mathscr{F}$, T and $|\mathscr{F} - T|$ are computed for the two belt tensioner models studied:

$$\max_{t\in[3,3.15]} |(\mathscr{F}(t) - T(t))/T(t)| = 4.36 \times 10^{-3},$$

$$\max_{t\in[3,3.15]} |(\mathscr{F}(t) - T(t))/\mathscr{F}(t)| = 4.34 \times 10^{-3}$$

for the MDM and

$$\max_{t\in[3,3.15]} |(\mathscr{F}(t) - T(t))/T(t)| = 4.42 \times 10^{-3},$$

$$\max_{t\in[3,3.15]} |(\mathscr{F}(t) - T(t))/\mathscr{F}(t)| = 4.40 \times 10^{-3}$$

for the MM with viscous damping. Thus it is considered that the value of $T(t)$ is roughly $\mathscr{F}(t)$. Therefore, each experimental value of $\mathscr{F}(t)$ is not measurable and it is then replaced by the corresponding experimental value $T(t)$.

After a short transient phase, functions $t\mapsto\mathscr{F}$, $t\mapsto u_1$ and $t\mapsto u_2$ are periodic. Thus, only some periods of these functions $t\mapsto\mathscr{F}$, $t\mapsto u_1$ and $t\mapsto u_2$ are plotted. Both measured and predicted results are presented in Figs. 17–19. The two theoretical models give satisfactory results. The short time deviation Δt is due to the unknown initial conditions. For the same reason, there are also shifts Δu_1 and Δu_2 between the experimental and computed curves u_1 and u_2; Δu_1 and Δu_2 are determined so that the mean values of u_1 and u_2 are nil. Finally, displacement shifts Δu_1, Δu_2 and Δt are introduced in the model and function $\mathscr{F}$ is plotted versus the deflection u_2 (see Fig. 20).

The comparisons of the results on Figs. 17–20 shows that there is a difference between the measured and predicted loops. The model parameters identification is performed for a low excitation pulsation due to the limitation of the experimental setup. Fig. 20 shows measured and predicted force-deflection loops conducted at the resonance frequency, which is eight times larger than the forcing frequency used for the parameter identification. Therefore, the discrepancy observed between measured and predicted loops is probably due to the inertia effects.

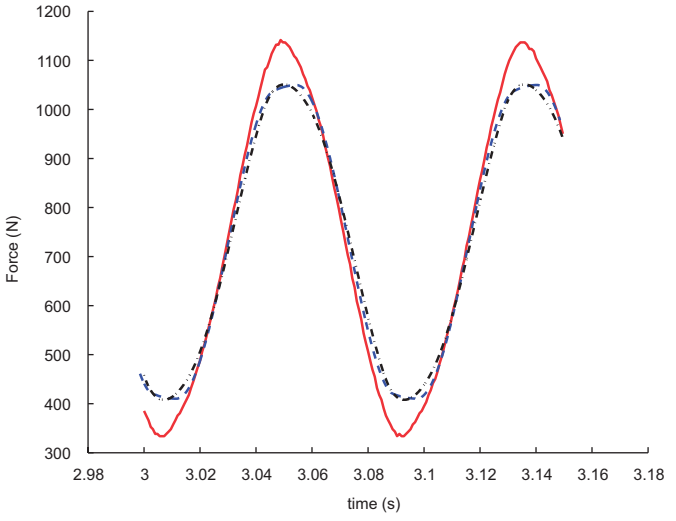

Fig. 17. Validation part: force $\mathscr{F}$ versus time measured (solid line) and predicted with the MDM (dashed line) and with the MM (dot-dashed line).

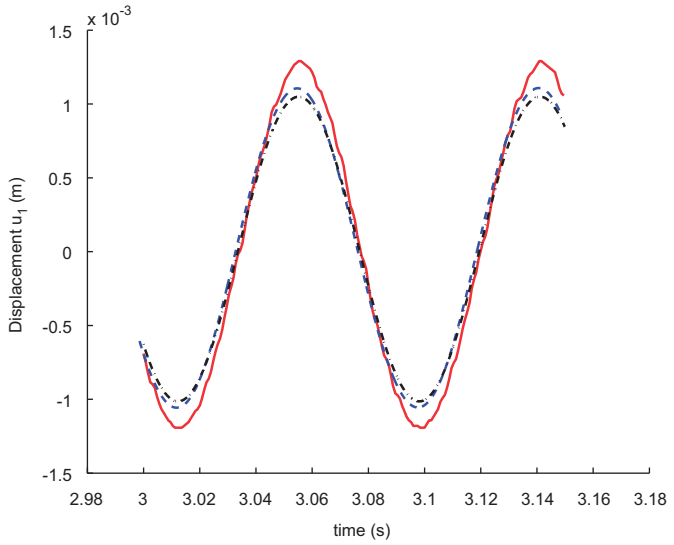

Fig. 18. Validation part: displacement u_1 versus time measured (solid line) and predicted with the MDM (dashed line) and with the MM (dot-dashed line).

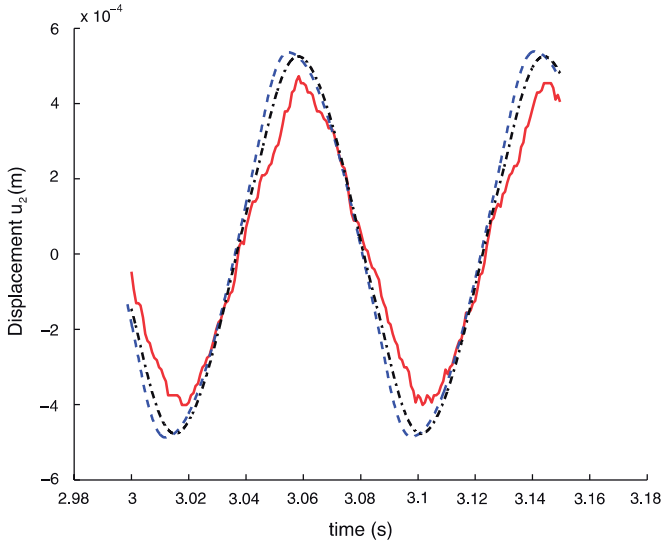

Fig. 19. Validation part: displacement u_2 versus the time measured (solid line) and predicted with the MDM (dashed line) and with the MM (dot-dashed line).

4.4. Global behavior

Finally, some values of $|\max(T) - \min(T)|$ versus forcing pulsation Ω are measured for several values of f_1 (and with f_0 and ϕ fixed) within Eq. (52). For each value of Ω, c_0 is defined by Eq. (31). We choose

$$t_0 = 17\,\text{s}, \quad t_f = 20\,\text{s}, \quad h = 10^{-5}\,\text{s}, \tag{59a}$$

$$f_0 = 0, \quad \phi = 0, \tag{59b}$$

$$f_1 \in [13, 27, 41, 54, 67, 79, 90, 100, 110, 120\,\text{N}], \tag{59c}$$

$$\Omega \in [10, 125\,\text{rad/s}] \text{ (with 116 values arranged linearly).} \tag{59d}$$

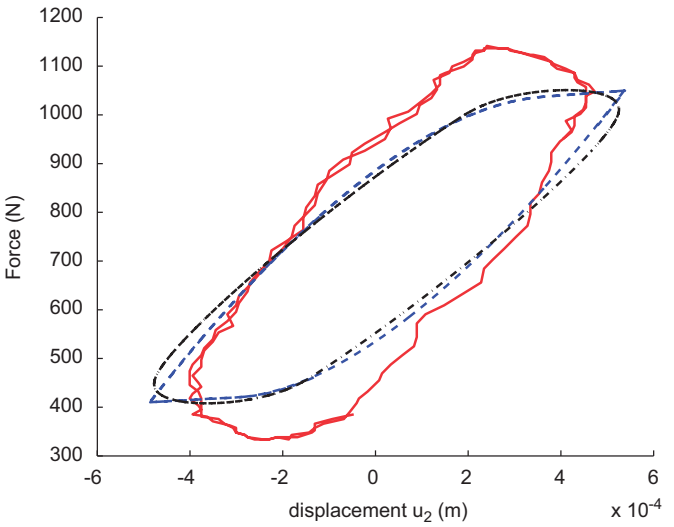

Fig. 20. Validation part: force $\mathscr{F}$ versus deflection u_2 predicted with the MDM (dashed line) with the MM (dot-dashed line), and measured (solid line).

Measured and predicted responses are plotted in Fig. 21. This figures gives the global behavior of the system. Experimentally, a resonant mode of the suspended shakers appears for low pulsation, and the used shaker does not permit applying higher forcing amplitude. The computed frequency response represented in this figure is obtained after a series of calculations in the time domain: each point of a frequency response curve corresponds to the tension fluctuation amplitude calculated when steady state is reached for a given frequency and excitation amplitude. The dot-dashed curves correspond to the predicted results obtained for higher excitation force amplitudes not provided by the experiment:

$$f_1 \in [140, 160, 200, 230, 260, 300\,\mathrm{N}]. \tag{60}$$

The global analysis of the three FRF graphs of Fig. 21 highlights different behavior depending on the forcing amplitude.

For small forcing amplitudes ($f_1 \in [0-30\,\mathrm{N}]$), the tensioner is stuck and equivalent to a spring-dashpot linear model with a high stiffness.

For high forcing amplitudes ($f_1 \in [200-300\,\mathrm{N}]$), the tensioner mainly slips and therefore could also be modeled by a spring-dashpot linear model with a low stiffness.

Between this two limit cases, the system exhibits a stick–slip motion where the resulting belt tension is bounded over a certain frequency range, also observed in Refs. [19,20]. The measured FRF, Fig. 21 (a), shows that the MDM reproduces quite well this threshold phenomenon.

Higher the forcing amplitude, greater nonlinear behavior becomes: for large forcing amplitudes ($f_1 > 200\,\mathrm{N}$), the FRF obtained with the MDM show a sub-harmonic phenomenon located at $\Omega = \omega_1(f_1)/3$, and an associated nonlinear softening resonance phenomenon where a jump occurs instead of the unstable branch.

5. Conclusion

Two hysteretic models have been analyzed and tested on a mechanical system containing a belt tensioner exhibiting a stick–slip behavior. The first model, which is the Masing model (MM) with viscous damping, provides, by the way of differential inclusion, the rheological parameters of the equation of motion. The second model, which is the modified Dahl model (MDM), recently proposed, provides a restoring force which takes place in the second member of the equation of motion. A primary experimental investigation carried out on the belt tensioner has permitted the model parameters identification. It sounds that the MM is enable to

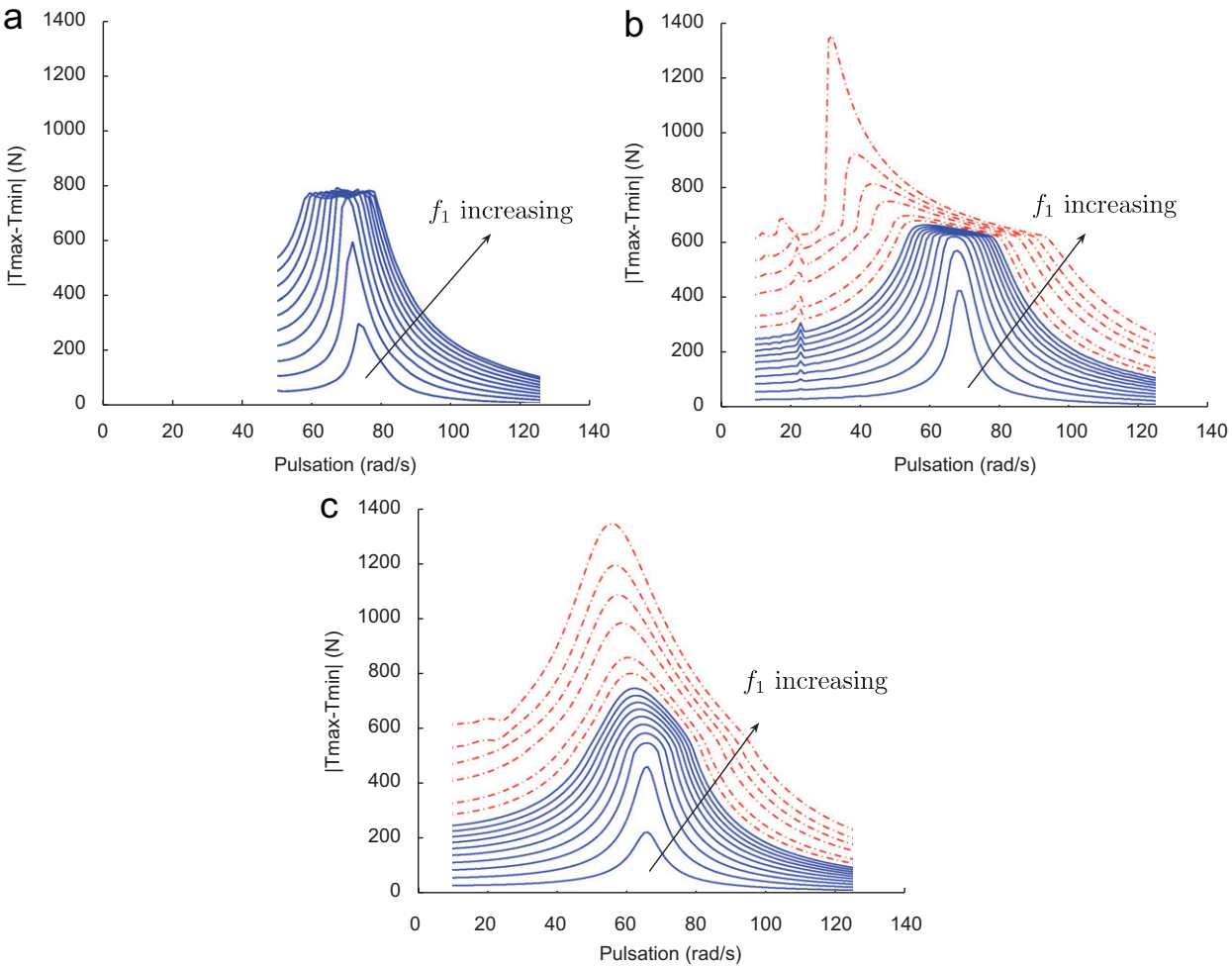

Fig. 21. Prediction part: amplitude $|\max(T) - \min(T)|$ versus pulsation Ω for several values of f_1 for the experiment (a), the MDM (b) and the MM with viscous damping (c) for f_1 defined by Eq. (59c) (solid curves) and for f_1 defined by Eq. (60) (dot-dashed curves), with f_1 increasing in the direction of the arrow.

reproduce better the transition from stick to slip motions observed on the measured force-deflection loops. In a second experiment, the FRF of a mass–belt–tensioner system highlights three different behaviors depending on the forcing amplitudes: higher the level, greater the nonlinear behavior becomes. The linear behavior corresponds to a stick state of the tensioner, while the nonlinear behavior which corresponds to a mainly slip state of the tensioner exhibit softening resonance phenomena associated to a subharmonic resonance. Using these two models for predicting FRF requires to carry out a time integration for each frequency step. It should be noticed that a particular attention must be paid to the use of the numerical schemes in order to make the predicted responses reliable. Regarding the measured response, the MDM shows a good efficiency especially for modeling the intermediate stick–slip state, where the belt tension level reaches a threshold.

Appendix A. A few theoretical reminders about the class of maximal monotone differential equations used

In this section, it is assumed that H is a Hilbert-space, equipped with a scalar product $<,>$ and its associated norm $|.|$. Let A be a multi-valued maximal monotone operator from H with domain $D(A)$ (see for example Ref. [18]).

A.1. Summary of existence and uniqueness result

In this section, we recall an existence and uniqueness result. Proof of this result can be found in Refs. [21,17]. It is assumed that f is a function from $[t_0, t_f] \times H$ to H, Lipschitz continuous with respect to its second argument and whose derivative maps the bounded sets of $L^2(t_0, t_f; H)$ into bounded sets of $L^2(t_0, t_f; H)$, i.e.,

$$\exists L \geqslant 0: \quad \forall t \in [t_0, t_f], \quad \forall x_1, x_2 \in H, \quad |f(t, x_1) - f(t, x_2)| \leqslant L|x_1 - x_2|, \tag{A.1}$$

and there exits a function Φ so that

$$\forall R \geqslant 0, \quad \Phi(R) = \sup\left\{ \left\| \frac{\partial f}{\partial t}(., v) \right\|_{L^2(t_0,t_f;H)} : \|v\|_{L^2(t_0,t_f;H)} \leqslant R \right\} < +\infty. \tag{A.2}$$

The existence and uniqueness result is developed in what follows.

Prosposition 1. *If u_0 belongs to $D(A)$, and if assumptions* (A.1) *and* (A.2) *hold, then there exists a unique solution $u \in W^{1,\infty}(t_0, t_f; H)$ of the differential inclusion*

$$\dot{u}(t) + A(u(t)) \ni f(t, u(t)), \text{ almost everywhere on } (t_0, t_f), \tag{A.3a}$$

$$u(t_0) = u_0. \tag{A.3b}$$

If ϕ is a convex proper and lower semi-continuous function from H to $(-\infty, +\infty)$, one can define its subdifferential $\partial\phi$ by

$$\begin{aligned} &y \in \partial\phi(x) \Longleftrightarrow \forall h \in \mathbb{R}^p, \quad \phi(x + h) - \phi(x) \geqslant \langle y, h \rangle, \\ &D(\partial\phi) = \{x : \partial\phi(x) \neq \emptyset\}; \end{aligned} \tag{A.4}$$

moreover, $\partial\phi$ is a maximal monotone graph in H. If Q is a closed convex non-empty subset of H, we denote by ψ_Q the indicatrix of Q defined by

$$\forall x \in H, \quad \psi_Q(x) = \begin{cases} 0 & \text{if } x \in Q, \\ +\infty & \text{if } x \notin Q. \end{cases} \tag{A.5}$$

In this particular case, $\partial\psi_Q$ which is the subdifferential of ψ_Q, is given by

$$\forall (x, y) \in Q \times H, \quad y \in \partial\psi_Q(x) \Longleftrightarrow \forall z \in Q, \quad \langle y, x - z \rangle \geqslant 0, \tag{A.6a}$$

and

$$\forall x \notin Q, \quad \partial\psi_Q(x) = \emptyset. \tag{A.6b}$$

The domain of the maximal monotone operator $\partial\psi_Q$ is equal to Q.

A.2. Summary of result for numerical schemes

In this section, the error estimation proved in Refs. [21,17] is recalled.

Let N be an integer, $h = (t_f - t_0)/N$ and U^p the solution of the numerical scheme

$$\forall p \in \{0, \ldots, N-1\}, \quad \frac{U^{p+1} - U^p}{h} + A(U^{p+1}) \ni f(t_0 + ph, U^p), \tag{A.7}$$

$$U^0 = u_0. \tag{A.8}$$

Solution U^p exists and is unique since A is maximal monotone; Indeed, in this case the operator $(I + hA)^{-1}$, where I is the identity of H, is a single-valued operator defined by the entire space H with U^{p+1} so that (see Ref. [18]):

$$\forall p \in \{0, \ldots, N-1\}, \quad U^{p+1} = (I + hA)^{-1}(hf(t_0 ph, U^p) + U^p). \tag{A.9}$$

Denote $u_h \in C^0([t_0, t_f], H)$ the linear interpolation at time $t_p = t_0 + hp$ of the solution U^p. The result of convergence is now detailed.

Prosposition 2. *Under the assumptions* (A.1) *and* (A.2), *if* ψ_Q *is defined by* (A.5) *and if* A *is equal to* $\partial\psi_Q$, *the numerical scheme* (A.7)–(A.8) *is of first order*, *i.e. there exists* C *so that*, *for any* h,

$$\forall t \in [t_0, t_f], \quad |u(t) - u_h(t)| \leqslant Ch, \tag{A.10}$$

where u *is the solution of* (A.3).

References

[1] W. Lacarbonara, F. Vestroni, Nonclassical responses of oscillators with hysteresis, *Nonlinear Dynamics* 32 (2003) 235–258.

[2] F. Vestroni, M. Noori, Hysteresis in mechanical systems—modeling and dynamic response, *International Journal of Non-Linear Mechanics* 37 (2002) 1261–1262.

[3] A. Visintin, *Differential Models of Hysteresis*, Springer, Berlin, 1994.

[4] J. Bastien, M. Schatzman, C.-H. Lamarque, Study of some rheological models with a finite number of degrees of freedom, *European Journal of Mechanics A—Solids* 19 (2) (2000) 277–307.

[5] R. Fougeres, F. Sidoroff, The evolutive masing model and its application to cyclic plasticity and ageing, *Nuclear Engineering and Design* 114 (1989) 273–284.

[6] A. Al Majid, R. Dufour, Formulation of a hysteretic restoring force model: application to vibration isolation, *Nonlinear Dynamics* 27 (2002) 69–85.

[7] A. Al Majid, R. Dufour, Harmonic response of a structure mounted on an isolator modelled with a hysteretic operator: experiment and prediction, *Journal of Sound and Vibration* 277 (2004) 391–403.

[8] R. Beikmann, N. Perkins, A. Ulsoy, Design and analysis of automotive belt drive systems for steady state performance, *ASME Journal of Mechanical Design* 119 (1997) 162–168.

[9] R. Parker, Efficient eigensolution, dynamic response, and eigensensitivity of serpentine belt drives, *Journal of Sound and Vibration* 270 (2004) 15–38.

[10] M. Leamy, N. Perkins, Nonlinear periodic response of engine accessory drives with dry friction tensioners, *ASME Journal of Vibration and Acoustics* 120 (1998) 909–916.

[11] P.-A.J. Bliman, Étude Mathématique d'un Modèle de Frottement Sec: Le Modèle de P.R. Dahl, PhD Thesis, Université de Paris IX-Dauphine, 1990.

[12] P.-A.J. Bliman, Mathematical study of the Dahl's friction model, *European Journal of Mechanics A—Solids* 11 (6) (1992) 835–848.

[13] G. Michon, L. Manin, R. Dufour, Hysteretic behavior of a belt tensioner: modeling and experimental investigation, *Journal of Vibration and Control* 11 (9) (2005) 1147–1158.

[14] A. Pokrovskiĭ, On the theory of hysteresis nonlinearities, *Soviet Mathematics Doklady* 14 (3) (1973) 896–900.

[15] M.D.P. Monteiro Marques, An existence uniqueness and regularity study of the dynamics of systems with one-dimensional friction, *European Journal of Mechanics A—Solids* 13 (2) (1994) 277–306.

[16] D.E. Stewart, Rigid-body dynamics with friction and impact, *SIAM Review* 42 (1) (2000) 3–39 (electronic).

[17] J. Bastien, M. Schatzman, Numerical precision for differential inclusions with uniqueness, *M2AN—Mathematical Modelling and Numerical Analysis* 36 (3) (2002) 427–460.

[18] H. Brezis, *Opérateurs Maximaux Monotones et Semi-groupes de Contractions dans les Espaces de Hilbert*, North-Holland Publishing Co., Amsterdam, 1973, (North-Holland Mathematics Studies, No. 5. Notas de Matemática (50)).

[19] F. D'Ambrosio, E. Chatelet, G. Jacquet, Influence of contact states on the dynamic behavior of rubbing structures, *Proceedings of IGTI 2005*, ASME Turbo Expo, Reno-Tahoe, Nevada, USA, 2005.

[20] K. Sanliturk, D. Ewins, Modelling two-dimensional friction contact and its application using harmonic balance method, *Journal of Sound and Vibration* 193 (2) (1996) 511–523.

[21] J. Bastien, M. Schatzman, Schéma numérique pour des inclusions différentielles avec terme maximal monotone, *Comptes Rendus de l'Académie des Sciences. Série I—Mathématique* 330 (7) (2000) 611–615.